

Demonstrating approaches to chemically modify the surface of Ag nanoparticles in order to influence their cytotoxicity and biodistribution after single dose acute intravenous administration

Chengfang Pang^{1,2}, Andrea Brunelli², Conghui Zhu¹, Danail Hristozov², Ying Liu³, Elena Semenzin², Wenwen Wang⁴, Wuqun Tao¹, Jingnan Liang⁵, Antonio Marcomini², Chunying Chen³, and Bin Zhao¹

¹State Key Laboratory of Environmental Chemistry and Ecotoxicology, Chinese Academy of Sciences, Beijing, P.R. China, ²Department of Environmental Sciences, Informatics and Statistics, University Ca' Foscari Venice, Venice, Italy, ³CAS Key Laboratory for Biomedical Effects of Nanomaterials & Nanosafety, National Center for Nanoscience and Technology of China, Beijing, P.R. China, ⁴Department of Physics, Beihang University, Beijing, P.R. China, and ⁵Core Facility of Equipment, Institute of Microbiology, Chinese Academy of Sciences, Beijing, P.R. China

Abstract

With the advance in material science and the need to diversify market applications, silver nanoparticles (AgNPs) are modified by different surface coatings. However, how these surface modifications influence the effects of AgNPs on human health is still largely unknown. We have evaluated the uptake, toxicity and pharmacokinetics of AgNPs coated with citrate, polyethylene glycol, polyvinyl pyrrolidone and branched polyethyleneimine (Citrate AgNPs, PEG AgNPs, PVP AgNPs and BPEI AgNPs, respectively). Our results demonstrated that the toxicity of AgNPs depends on the intracellular localization that was highly dependent on the surface charge. BPEI AgNPs (potential +46.5 mV) induced the highest cytotoxicity and DNA fragmentation in Hepa1c1c7. In addition, it showed the highest damage to the nucleus of liver cells in the exposed mice, which is associated with a high accumulation in liver tissues. The PEG AgNPs (potential 16.2 mV) showed the cytotoxicity, a long blood circulation, as well as bioaccumulation in spleen (34.33 mg/g), which suggest better biocompatibility compared to the other chemically modified AgNPs. Moreover, the adsorption ability with bovine serum albumin revealed that the PEG surface of AgNPs has an optimal biological inertia and can effectively resist opsonization or non-specific binding to protein in mice. The overall results indicated that the biodistribution of AgNPs was significantly dependent on surface chemistry: BPEI AgNPs > Citrate AgNPs > PVP AgNPs > PEG AgNPs. This toxicological data could be useful in supporting the development of safe AgNPs for consumer products and drug delivery applications.

Keywords

Acute toxicity, pharmacokinetics, protein adsorption, surface coating

Introduction

Nanotechnology is one of the key emerging technologies and has enormous potential to contribute to innovation, which fosters large investments in developing new industrial applications. This is reflected in the increasing number of nanotechnology-based products that reach the market (Nanodb.dk). However, our understanding of the potential environmental, health and safety risks of manufactured nanomaterials (NMs) is still limited, which may result in stagnation of nano-innovation.

Silver nanoparticles (AgNPs) are finding various applications in medical devices, diagnosis and therapeutics and antiparasitic efficacy, and drug delivery for life-threatening diseases (Holder et al., 2003). With the increasing application of AgNPs in medical devices and products, there are growing concerns about the health and ecological risks upon release into the environment. A number of studies have shown that AgNPs can be taken up by living organisms, where they migrate to the liver, spleen, lungs, kidneys and brain to induce apoptosis, membrane damage, inflammation and DNA damage (Gliga et al., 2014; Mahmood et al., 2010; Sharma et al., 2014; Suliman et al., 2015; Yang et al., 2012; Yin et al., 2013; Yu et al., 2013). These data have demonstrated that reactive oxygen species, oxidative stress and modified inflammatory responses play an important role in its animal and cellular toxicity (Chen et al., 2014; Farkas et al., 2011; Singh & Ramarao, 2012; Walkey et al., 2014; Xue et al., 2012; Yin et al., 2013; Yu et al., 2013).

With the advance in material science, AgNPs with different surface coating were exploited to develop more sensitive diagnostic agents for medical imaging and carrier substance for cancer, e.g. polyvinyl pyrrolidone-coated AgNPs (PVP AgNPs) were most effective for inhibition of Human Immunodeficiency Virus replication (Trefry & Dawn, 2013); branched polyethyleneimine has been used to coat and deliver poly(L-lactic-co-glycolic acid) nanoparticles (NPs) into stem cells (Kim et al., 2011b; Park et al., 2010, 2013); and polyethylene glycol coating can increase the *in vivo* half-life of drug components (Majzoubet al., 2014). However, the coating of AgNP surface with different agents may lead to complex nano-bio interactions causing toxicity in cells or organisms. In fact, since the toxicity of NMs is mainly driven by factors such as particle size, composition, surface coating, shape, surface charge, aggregation and released ions (Gaiser et al., 2013; Gliga et al., 2014; Lee et al., 2014; Panget al., 2012, 2013; Qiu et al., 2010; Sahu et al., 2014; Wang et al., 2013; Zhang et al., 2014), a slight change in AgNPs size or surface chemistry may dramatically influence its physiological response. For example, Gliga et al. showed that the AgNPs toxicity in human lung cells is associated with the rate of intracellular Ag release, which depends on the size of the AgNPs (Gliga et al., 2014). Apart from the size of NPs, their surface chemistry/amphiphilicity is largely responsible for their *in vivo* fate because it determines the amount of adsorbed serum components, mainly proteins (Fleischer & Payne, 2014; Treuelet al., 2014; Verma & Stellacci, 2010).

From an extensive literature review, it appears that most toxicological studies focus on few coated AgNPs, such as PVP AgNPs or citrate-coated AgNPs (Citrate AgNPs), looking mainly at the effects of their size (distribution) on toxicity (Gliga et al., 2014; Massarsky et al., 2013; Xue et al., 2012; Yu et al., 2013; Zhang et al., 2013). To date, a comprehensive understanding of the influence of AgNPs surface coatings on cell uptake and pharmacokinetics is still lacking, which could support the safe design of AgNP-based products for consumers and medical applications. To address this issue, for the first time we evaluated the uptake, biodistribution and toxicity of four different types of organic-coated AgNPs, namely Citrate AgNPs, polyethylene glycol (PEG AgNPs), PVP AgNPs and branched polyethyleneimine-coated AgNPs (BPEI AgNPs) in Balb/c mice and mouse hepatoma cells (Hepa1c1c7).

Methods

Characterization of AgNPs

Commercially relevant AgNPs (Citrate AgNPs, PEG AgNPs, PVP AgNPs and BPEI AgNPs) were purchased as dispersions from the nanoComposix Company (San Diego, CA). The AgNO₃ (CAS No. 7761880) material was purchased from Sigma-Aldrich (St. Louis, MO). The endotoxin concentration in the four AgNPs stock suspensions was tested using the Kinetic Turbidity Assay (NCL Method STE-1.2). The AgNPs diameter was determined by transmission electron microscopy (TEM, JEOL 1010, Tokyo, Japan) followed by statistical examination, i.e. analysis of variance (ANOVA). Inductively coupled plasma mass spectrometry (ICP-MS, Thermo Fisher X Series 2, Waltham, MA) was used to measure the mass concentration and corresponding particle number concentration of the Ag stock solutions. ICP-MS was also used to determine Ag⁺. The total mass of capping ligand in each solution was estimated by assuming a 5-nm-thick layer of polymeric capping ligand (PEG, PVP, BPEI) on each particle and a 0.5-nm-thick layer of molecular citrate (NanoComposix). Spectral properties were investigated by UV-Visible Spectrophotometer (Agilent 8453, Agilent Technologies, Inc., Santa Clara, CA). Hydrodynamic diameter and potential were measured by Zetasizer Nano ZS (Malvern Instruments Ltd., Worcestershire, UK).

Cell lines and cell culture

Hepa1c1c7 were provided by the Department of Environmental Toxicology, University of California, Davis and maintained at 37 °C in incubator with a humidified atmosphere of 5% CO₂ and cultured in cell culture plates in Minimum Essential Media a (Gibco®) with 10% fetal bovine serum (Gibco®) (Invitrogen Corporation, Carlsbad, CA) and antibiotics.

Cell viability

Cell viability was measured by the CellTiter-Glo® luminescent cell viability assay (Promega, Madison, WI). The experiments were performed in white opaque-walled 96-well plates (Nunc, Myriad Industries, San Diego, CA). For the ATP assay, 5 × 10³ cells per well were plated and treated with different concentration (0, 0.1, 1, 5, 10, 25 and 50 mg/ml) of citrate AgNPs, PVP AgNPs, PEG AgNPs, BPEI AgNPs and AgNO₃ for 24 h, respectively.

AgNPs uptake and TEM-energy dispersive X-ray spectroscopy analysis of Hepa1c1c7 cells

According to the EC₅₀ values obtained from the cell viability testing, 5 mg/ml, resulting in around 80% cell viability, was chosen as the exposure concentration of AgNPs uptake and molecular toxicity. After exposing the cells to 5 mg/ml of Citrate AgNPs, PEG AgNPs, PVP AgNPs, BPEI AgNPs and AgNO₃ for 24 h in six-well plates, respectively, the cells were sampled by detachment with Trypsin and digested (HNO₃-H₂O₂ 3:1) in a microwave oven (Milestone MLS-1200 Mega, Leutenkirch, Germany). The digestion program was 250, 400, 650 and 250 W for 6 min, respectively. After cooling, the digestion solution was filtered and measured by ICP-MS for determining AgNPs uptake by cells.

In order to study the intracellular localization of AgNPs, the cells were treated in the same way as in the uptake study explained above. The cells were pre-fixed in 2.5% glutaraldehyde in 0.1 M sodium phosphate buffer, pH 7.2 for 6 h at room temperature (RT) followed by a thorough wash with phosphate buffer. Fixed materials were exposed after fixation to 1% aqueous osmium tetroxide for 2 h at RT. Dehydration of samples was achieved by transferring to vials containing a graded water–acetone series (10% steps for 30–90% each of 15 min, 100% for 30 min). Dehydrated specimens were embedded with Epon 812 and then polymerized in Spurr's resin (Epon 812 with 1.5% hardening agent, DMP30) at 45 °C for 24 h and 65 °C for 72 h. Thin sections (80 nm thickness) were prepared using a Leica UC 7 (Wetzlar, Germany) on 100 mesh grids and then examined under a JEM-1400 TEM (Peabody, MA) after treatment with uranyl acetate for 20 min and with lead citrate for 5 min. The detected AgNPs or Ag⁺ in cells were analyzed by energy dispersive X-ray (EDX) spectroscopy.

Total RNA extraction and reverse transcription-polymerase chain reaction analysis

Total RNAs were isolated from cells using Trizol[®] reagent (Invitrogen, Carlsbad, CA) following the treatment of cells over 24 h with Citrate AgNPs, PEG AgNPs, PVP AgNPs, BPEI AgNPs and AgNO₃ at the concentration of 5 mg/ml. Apoptotic genes (Bcl 2 and Caspase 3) were detected by reverse transcription-polymerase chain reaction (RT-PCR), where housekeeping b-actin gene was used as internal control. Real time RT-PCR analysis was performed with Roche Light Cycler (Mannheim, Germany) using the Takara SYBR Premix ExTaq system (Otsu, Japan). The PCR program cycles were set as 40 cycles of 94 °C for 30 s, 57 °C for 60 s and 72 °C for 60 s, for each coated AgNP. Primers were synthesized by Life Technology (Beijing, China) and primer sequences are: Bcl 2, 5'-AGA GGG GCT ACG AGT GGG AT-3', 3'-CTC AGT CAT CCA CAG GGC GA-5'; Caspase 3, 5'-AGT CAG TGG ACT CTG GGA TC-3', 3'-GTA CAG TTC TTT CGT GAG CA-5'; b-actin, 5'-ATC CGT AAA GAC CTC TAT GC-3', 3'-AAC GCA GCT CAG TAA CAG TC-5'. Gene expression was determined by RT-PCR and normalized against b-actin mRNA levels.

DNA fragmentation

The APO-BRDU kit (Phoenix Flow Systems, San Diego, CA), detecting DNA strand breaks *in situ* by labeling them with fluorochromes, was used to identify apoptotic cells. Hepa1c1c7 cells were exposed to Citrate AgNPs, PEG AgNPs, PVP AgNPs, BPEI AgNPs and AgNO₃ at concentration of 5 mg/ml each. After 24 h, the cells were suspended in 1 PBS (pH 7.4) and fixed in 1% (w/v) paraformaldehyde in PBS at a concentration of 1 × 10⁶ cells/ml. The cell suspension was washed in PBS, centrifuged twice, then adjusted to 1 × 10⁶ cells/ml in 70% (v/v) ice-cold ethanol and stored 12 h at 20 °C. Ethanol-fixed cells were washed twice with wash buffer and supernatant was discharged by centrifugation. Freshly prepared DNA labeling solution (containing TdT and Br-dUTP) was added to the cell pellet and incubated for 1 h at 37 °C with occasional shaking. Cells were labeled by FITC-conjugated mAbs to BrdU, washed again and resuspended in staining solution containing PI and RNase. Cells were incubated for 30 min at RT and immediately analyzed using FACS Calibur flow cytometer and CELL-Quest software (BD Biosciences, San Jose, CA).

Animal exposure

Eight-week-old male Balb/c mice were provided by Vital River Laboratories (Vital River Co., Beijing, China) and were acclimated to the environment for a week prior to dosing. The mice were intravenously injected as follows: 200 µl 0.9% physiological saline solution (Double Crane Pharmaceutical Co., Ltd., Beijing, China) at the control group; 200 µl of Citrate AgNPs, PEG AgNPs, PVP AgNPs, BPEI AgNPs suspensions; 200 µl AgNO₃ solution at 100 mg Ag/ml (corresponding to doses of 1 mg/kg which was diluted by stock concentration of 1 mg/ml, 20 mg Ag per mouse, 5 mice per group per time course). The mice were sacrificed and organs were collected after 24 h for chemical analysis. The animal experiment was performed in compliance with the local ethics committee and the Guideline for the Care and Use of Research Animals.

Biodistribution analysis

Ag biodistribution based on the quantification of ¹⁰⁷Ag (the highest relative abundant in Ag) in tissues was analyzed by ICP-MS. The collected organs including liver, spleen, lung, kidney, intestine and brain were weighed and transferred to a wellon tube. The samples were digested with 8 ml of HNO₃:H₂O₂ 3:1 in a microwave oven (Milestone MLS-1200 Mega). The digestion program was 250, 400, 650 and 250 W for 6 min. After cooling, the digestion solution was filtered and measured by ICP-MS.

Pharmacokinetics analysis

Blood was collected from mice at different time points (2 min, 10 min, 30 min, 60 min, 6 h, 12 h, 24 h and 72 h) for pharmacokinetics analysis. The content of Ag in blood was measured by ICP-MS as described above.

Ability of AgNPs to adsorb bovine serum albumin

The ability of AgNPs with different surface coatings to adsorb bovine serum albumin (BSA) was tested by bicinchoninic acid (BCA) Protein Assay Reagent (Pierce, Rockford, IL). A homogeneous solution of BSA with each AgNP was made and kept at RT for 1 h. The mixed suspensions were centrifuged. The supernatants were transferred to wells of a 96-well plate and the concentrations of BSA were measured by BCA Protein Assay Reagent (Pierce, Rockford, IL), using a plate reader at A562.

Statistical analysis

AgNPs uptake by cells, gene expression and adsorption of BSA were analyzed by SPSS version 16 (Chicago, IL) by one-way ANOVA followed by Tukey's test, $p \leq 0.05$ was considered significant. Prior to ANOVA, Levene's test was used to check homogeneity of variances. The pharmacokinetic parameters of various AgNPs and Ag^+ in the blood were analyzed through WinNonLin version 5.2 (Pharsight, Princeton, NJ).

Results

Characterization of AgNPs

TEM images showed that all the investigated AgNPs were monodispersed with similar primary size (around 30 nm) (Figure 1). The four kinds of AgNPs showed different potential values, varying from 22.9 to +46.5 mV (Table 1). The hydrodynamic size of all AgNPs showed that the stock suspensions were stable in Milli-Q water media. The concentration of each capping ligand and the Ag^+ and the content of endotoxin in stock suspension are shown in Table 1.

Cell viability and intracellular localization of AgNPs in Hepa1c1c7

ATP assays to assess the toxicity of Citrate AgNPs, PEG AgNPs, PVP AgNPs, BPEI AgNPs and Ag^+ to Hepa1c1c7 cells showed that BPEI AgNPs showed very high toxicity (EC_{50} 10.38 mg/ml). However, PEG AgNPs-treated cells showed the lowest toxicity (EC_{50} 63.14 mg/ml) and the lowest uptake among all AgNPs treatments ($p \leq 0.05$) (Figures 2B and 3C). The highest uptake for BPEI AgNPs was 3.25 pg/cell, which was three times greater than PEG AgNPs uptake (1.02 pg/cell) (all concentrations in the study were calculated as Ag concentration).

Intracellular localization imaging showed that Citrate AgNPs, PVP AgNPs and BPEI AgNPs were taken up mainly within membrane-bound structures (Figure 3A). Nuclear localization for BPEI AgNPs was detected by TEM-EDX imaging confirming the highest uptake of BPEI AgNPs in Hepa1c1c7 (Figure 3A and B). Ag^+ (source from AgNO_3) was measured in order to be compared with AgNPs. Both the imaging of intracellular localization and the cellular dose of Ag^+ in Hepa1c1c7 demonstrated that the uptake of Ag^+ was much lower than the uptake of AgNPs in Hepa1c1c7 (Figure 3A and C).

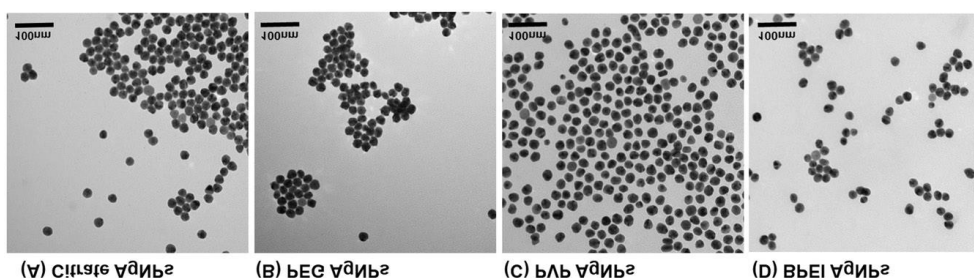


Figure 1. TEM images of AgNP in stock suspensions: (A) Citrate AgNPs, (B) PEG AgNPs, (C) PVP AgNPs and (D) BPEI AgNPs.

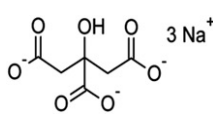
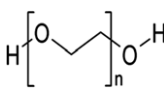
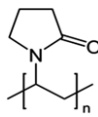
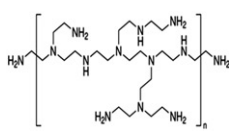
DNA fragmentation and gene expression differences

The APO-BRDU kit detection of DNA strand breaks showed that only BPEI AgNPs-treated cells showed DNA fragmentation (13.2%) (Figure 4A). Caspase 3 gene expression after Ag^+ treatment was significantly up-regulated compared to control and other AgNPs treatments ($p \leq 0.05$) (Figure 4B). Bcl 2 gene expression was significantly lower after treatment with Citrate AgNPs, PVP AgNPs and BPEI AgNPs treatments compared to controls ($p \leq 0.05$) (Figure 4C).

Biodistribution of AgNPs in mice

The biodistribution results showed that total Ag was higher in spleen and liver, followed in a decreasing order by lungs, gut, kidneys and brain (Figure 5). The mice treated with BPEI AgNPs showed much higher body burden in lung compared to the AgNPs and Ag^+ treatments ($p \leq 0.05$). However, the mice treated with PEG AgNPs showed very high body burden in spleen (34.33 mg Ag/g spleen; 2.06 mg per mouse spleen, Figure 5).

Table 1. Physicochemical properties of Citrate AgNPs, PEG AgNPs, PVP AgNPs and BPEI AgNPs, as well as Ag⁺ concentration in stock suspensions.

Name	TEM size (nm) (SD)	Hydrodynamic size (nm) Average (SD)	Zeta potential (mV)	Mass conc. (mg/ml)	Particle conc. (particles/ml)	Capping ligand (mg/ml)	Particles surface	pH	Solvent	Endotoxin (EU/ml)	Ag ⁺ conc. (mg/l)
Citrate AgNPs	28.7 (3.6)	35.8 (3.1)	-22.9	1.14	7.7E+12	0.017		7.1	Aqueous 2 nM Citrate	0.50	0.43 (0.10)
PEG AgNPs	32.9 (3.2)	54.6 (4.4)	-16.2	1.08	5.6E+12	0.160		6.5	Milli-Q water	0.69	0.45 (0.03)
PVP AgNPs	28.7 (2.1)	36.2 (3.0)	-22.1	1.07	7.7E+12	0.160		6.4	Milli-Q water	0.04	0.58 (0.10)
BPEI AgNPs	30.0 (3.0)	63.0 (3.6)	46.5	0.49	2.5E+12	0.066		8.1	Milli-Q water	0.36	0.80 (0.07)

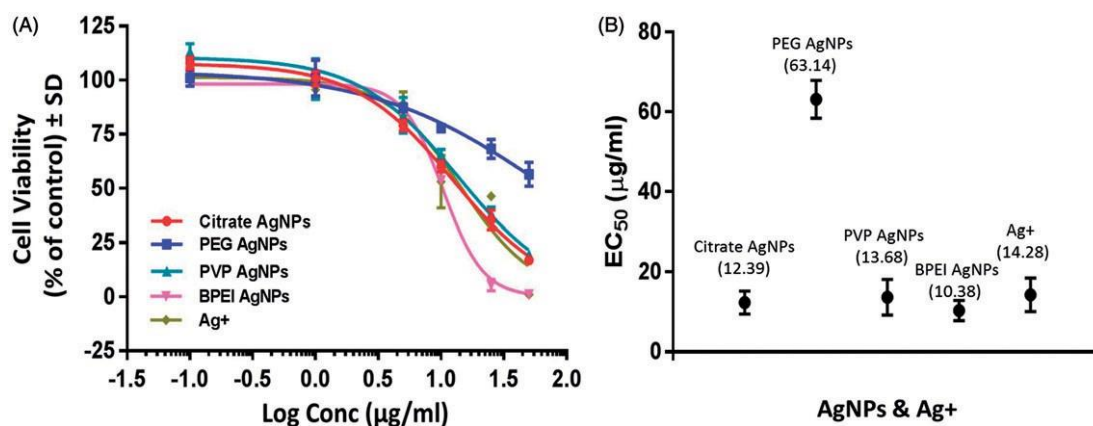


Figure 2. (A) Cell viability of AgNPs in Hepa1c7 cells treated with 5 mg/ml Citrate AgNPs, PEG AgNPs, PVP AgNPs, BPEI AgNPs and Ag⁺ for 24 h. (B) The EC₅₀ values were determined using the software GraphPad Prism 6. Data are shown as plots of the mean EC₅₀ of cell viability of various AgNPs and Ag⁺.

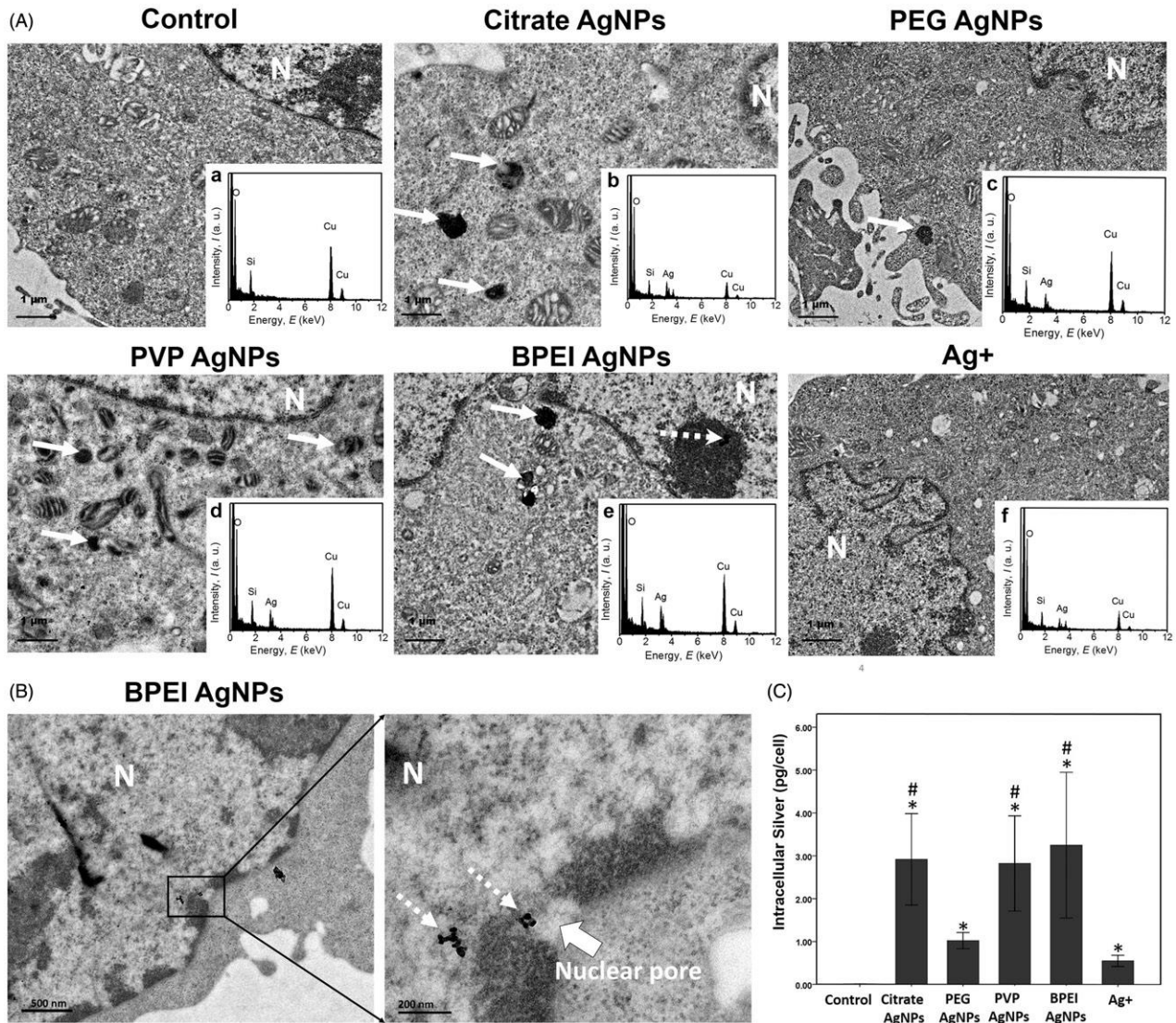


Figure 3. (A) Intracellular localization of AgNPs in Hepa1c1c7 cells. Citrate AgNPs, PVP AgNPs and BPEI AgNPs are taken up and mainly within membrane-bound structures (white solid arrow). BPEI AgNPs were observed in the nucleus (white dotted arrow). N indicates the nucleus. (a–f) Energy dispersive X-ray spectroscopy analysis to the uptake AgNPs in cells. (B) BPEI AgNPs entered into the nucleus through nuclear pores. (C) Ag concentration in Hepa1c1c7 cells. The cellular Ag accumulation was quantified by ICP-MS. The Ag content was expressed as pg per cell. Results are presented as mean \pm standard deviation of four replicates. The asterisks * p \leq 0.05 comparing the untreated and treated (AgNPs, Ag+) cells. # p \leq 0.05 comparing all treated (AgNPs and Ag+) cells.

Pharmacokinetics of AgNPs in mice and adsorption BSA ability of AgNPs

The pharmacokinetics profile of time and total Ag in blood is presented in Figure 6(A) showing a different trend between PEG AgNPs and other AgNPs and Ag⁺. A two-compartment model was found to fit the pharmacokinetics of Citrate AgNPs, PVP AgNPs, BPEI AgNPs and Ag⁺. PEG AgNPs treatment was fitted to a non-compartment model. The model choice was identified by the Akaike Information Criterion and the goodness of fit (Supplementary Figure S5) (Bachler et al., 2013). The pharmacokinetic parameters [including area under curve (AUC), half-life, clearance (CL) and volume of distribution (V)] were estimated and are presented in Table 2. The elimination half-life of PEG AgNPs in blood was much higher than other AgNPs and Ag⁺ treatments. Furthermore, the AUC was also higher in PEG AgNPs, which was 2, 6, 8 and 4 times higher than in Citrate AgNPs, PVP AgNPs, BPEI AgNPs and Ag⁺, respectively. The BSA adsorption ability of AgNPs with different surface coating indicates that PEG AgNPs showed lower protein adsorption than other AgNPs (p \leq 0.05) (Figure 6B).

Discussion

Characterization of AgNPs

TEM images showed similar size of the AgNPs used in our study, which indicated that the differences in toxicity to cells and mice was not due to size. The spectral properties and hydrodynamic size distribution further supported this conclusion (Supplementary Figure S1). The four kinds of AgNPs showed different potential values, which varied from -22.9 to +46.5 mV (Table 1), playing an important role in our toxicity studies. The content of endotoxin in Citrate AgNPs, PVP AgNPs and BPEI AgNPs was lower than the maximum acceptable endotoxin level of 0.5 EU/ml (FAD, USA) (Table 1). The content of endotoxin in PEG AgNPs was the highest (0.69 EU/ml) and therefore it was decreased for exposure experiment to a value (50.069 EU/ml) below the acceptable level. The low endotoxin content indicates that there is no contribution of bacterial to the toxicity of AgNPs *in vivo* and *in vitro*.

The relationship of toxicity and intracellular localization of AgNPs in Hepa1c1c7

ATP assays to assess the toxicity of Citrate AgNPs, PEG AgNPs, PVP AgNPs, BPEI AgNPs and Ag⁺ to Hepa1c1c7 cells showed that the cell viability was both concentration and surface coating dependent (Figure 2). The EC₅₀ of BPEI AgNPs was almost six times higher than for other AgNPs (Figure 2B). This result was consistent with cell morphology results (Supplementary Figure S2). The uptake of PEG AgNPs was much lower than for other AgNPs and Ag⁺. The lowest uptake of PEG AgNPs by cells may be due to the PEG coating that can reduce electrostatic interaction with cell plasma membrane, resulting in inefficient uptake (Gao et al., 2013; Majzoub et al., 2014). This result was consistent with the PEG coating with slightly negative charge, reducing the non-specific uptake by liver and spleen *in vivo* to some extent attributed to the electrostatic repulsion between negatively charged micelles (PEG coating) and the cellular surface (Yamamoto et al., 2001).

Combining data on the pharmacokinetics of PEG AgNPs in blood of mice (Figure 6A), the low uptake by cells and long circulation in blood of PEG AgNPs ($t_{1/2}$ 51.65 h, Table 2) indicated that PEG AgNPs can represent the best choice (among the four investigated coated AgNPs) in biomedical applications as drug delivery nanocarriers in cancer therapy.

Furthermore, the nuclear localization of BPEI AgNPs was detected by TEM-EDX, and this is in line with the highest uptake of BPEI AgNPs found in Hepa1c1c7 (Figure 3). Similar results were found for the AuNPs with Caco-2 cells (Liang et al., 2010) and BENS-2B cells (Kim et al., 2011a). The fact that BPEI AgNPs entered into nuclear may be due to the interplay between the higher positive surface charge of BPEI AgNPs and the nucleus membranes. As an effective transfection carrier for gene delivery, polyethylenimine (PEI) has been used to coat and deliver poly(L-lactic-co-glycolic acid) NPs into stem cells, enabling the endosomal escape of the particles and their release into the cytoplasm, followed by their re-entry into the nucleus of stem cells (Kim et al., 2011b; Park et al., 2010, 2013). As a kind of PEI, BPEI coating on AgNPs also showed a similar ability to re-entering the nucleus. However, our toxicity results indicated that BPEI AgNPs are not a good option for gene delivery because of their high cell toxicity and DNA damage to Hepa1c1c7 (Figures 2 and 4A).

Since the release of Ag⁺ plays an important role in the toxicity of AgNPs (Jiang et al., 2014; Lubick, 2008), Ag⁺ (source from AgNO₃) was measured as a comparison to AgNPs. Both the imaging of intracellular localization and cellular dose of Ag⁺ in Hepa1c1c7 demonstrated that the uptake of Ag⁺ was much lower than the uptake of AgNPs in Hepa1c1c7 (Figure 3A and C). Similar results were already published, showing that the uptake of AgNPs was higher than the uptake of Ag⁺ in human lung cells, A549 and BEAS-2B cells (Cronholm et al., 2013; Gliga et al., 2014). AgNPs toxicity studies suggested that a so-called Trojan-horse mechanism plays an important role in the toxicity of AgNPs. In fact, AgNPs can be taken up by the cells followed by release of Ag⁺, which is assumed to generate excess free radicals within the cells and oxidative stress-mediated pathways leading to cell death (Jiang et al., 2013; Lubick, 2008). Therefore, the lowest toxicity of Ag⁺ at the lowest exposure concentrations may be due to a lower uptake of Ag⁺ in Hepa1c1c7 (Figures 2 and 3). However, the significant toxicity of Ag⁺ to Hepa1c1c7 at higher exposure concentrations suggested that the toxicity mechanisms of Ag⁺ may differ from AgNPs. This assumption was supported by the gene expression study (Figure 4).

The expression of Caspase 3 in Ag⁺ treatment was significantly up-regulated compared to control and other AgNP treatments ($p < 0.05$) (Figure 4B). The results demonstrated that AgNPs may cause apoptosis via a distinct pathway from that of Ag⁺, thus inducing different toxicity to Hepa1c1c7 which suggested the AgNPs toxicity was not only linked to its chemical composition, but also to other physicochemical properties (i.e. surface coating). This is confirmed by some studies using the human lung epithelial cell line A549 and Jurkat T cell (Eom et al., 2014; Foldbjerg et al., 2012). Bcl 2 gene expression was significantly lower in Citrate AgNP, PVP AgNP and BPEI AgNP treatments than in the control ($p < 0.05$) (Figure 4C). The highest loss of mitochondrial membrane potential was observed for BPEI AgNPs (59.9%) among all AgNP treatments, the Ag⁺ treatment and the control ($p < 0.05$) (Supplementary Figure S3). The results suggest that the apoptosis mechanisms of AgNPs were also surface coating dependent, which make the AgNPs toxicity more complicated. This issue needs to be further studied in detail by determining the global gene expression after exposure to cells to AgNPs with different surface coating.

DNA fragmentation results showed that only BPEI AgNPs-treated cells presented DNA fragmentation (13.2%) (Figure 4A). This result was consistent with the intracellular localization of BPEI AgNPs in the nucleus. The DNA fragmentation may be due to the positive charge of BPEI AgNPs, which is directly interacting with chromatin when BPEI AgNPs enters the nucleus. However, other studies showed that PVP AgNPs and Citrated AgNPs-induced DNA damage in human lung cells at a concentration of 10 mg/ml (Gliga et al., 2014). Kovvuru et al. also showed that PVP AgNPs induced large DNA deletions in developing embryos,

irreversible chromosomal damage in bone marrow and double strand breaks and oxidative DNA damage in peripheral blood and/or bone marrow (Kovvuru et al., 2014). The absence of DNA damage in PVP AgNPs- and Citrate AgNPs- treated cells in our study may be due to its lower concentration(5 mg/ml) and the use of different cell lines. Therefore, multiple factors like surface coating, size, concentration and cell type should be considered in evaluating AgNPs toxicity.

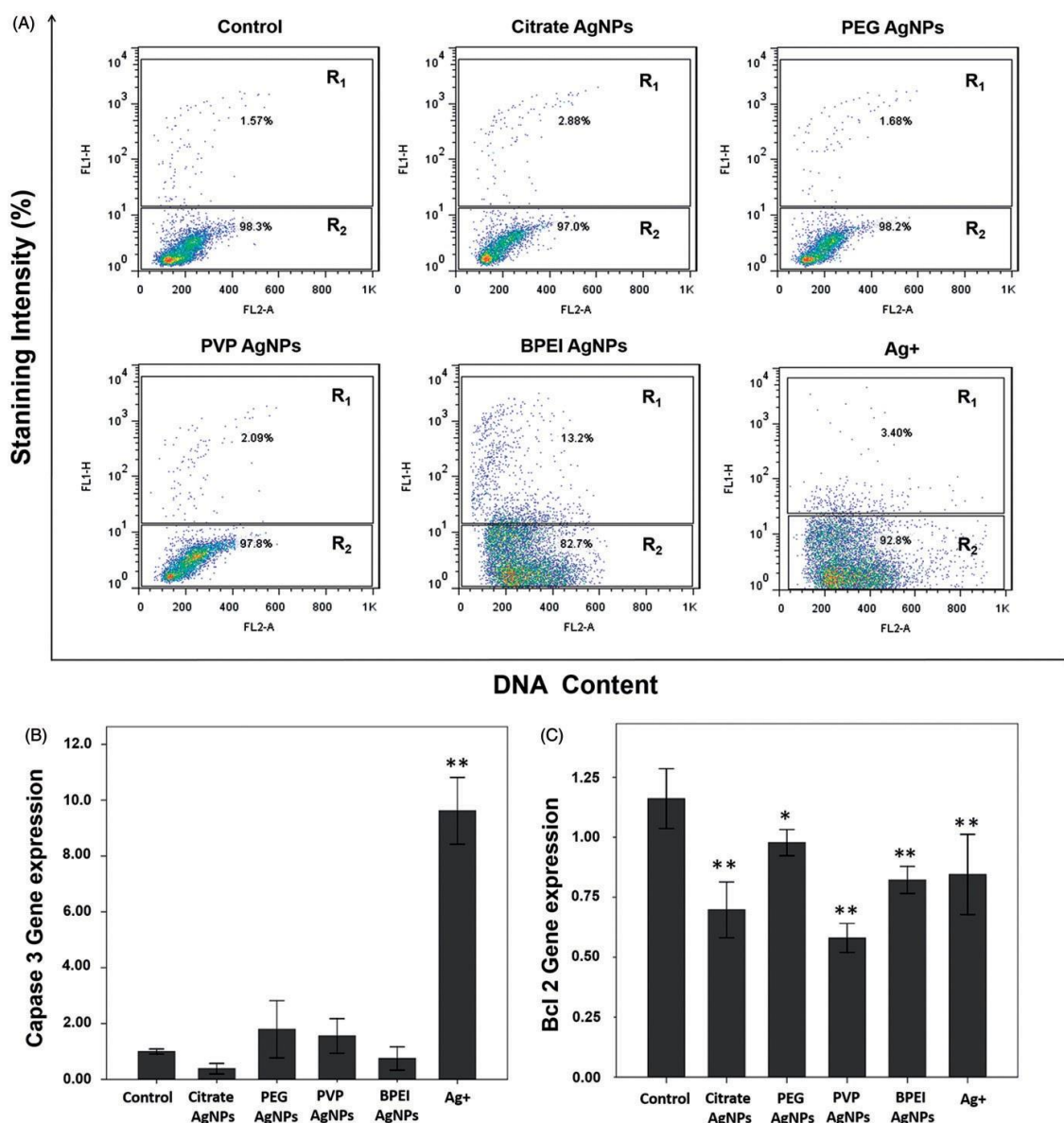
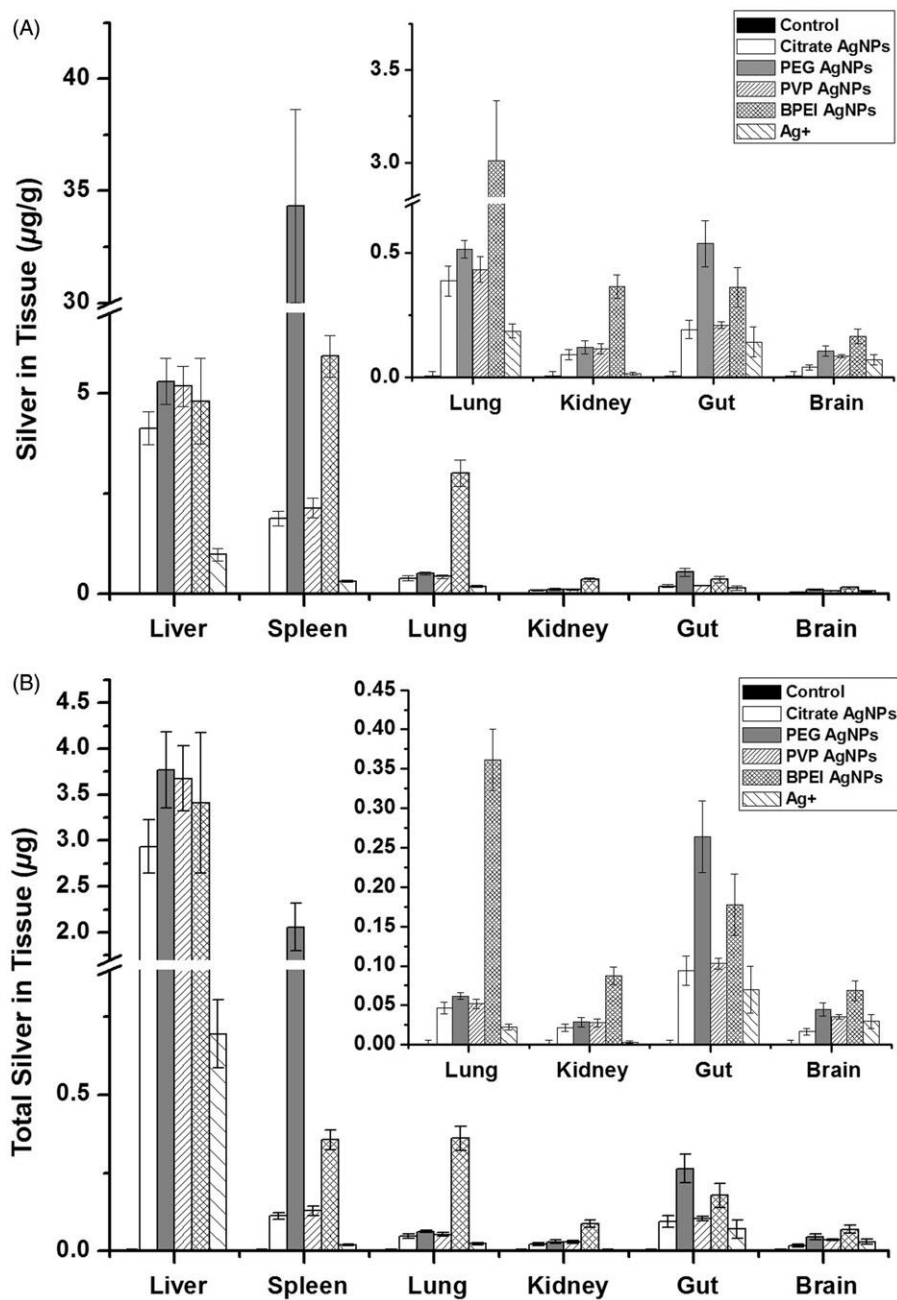


Figure 4. The apoptosis mechanisms of Hepa1c1c7 induced by AgNPs at 24 h post-exposure to Citrate AgNPs, PEG AgNPs, PVP AgNPs, BPEI AgNPs and Ag+ with 5 mg/ml concentration. (A) Flow cytometric analysis of DNA fragmentation in Hepa1c1c7 cells. The percentage of apoptotic cells was determined by TUNEL assay followed by flow cytometry analysis. The x-axis represents DNA content and the y-axis represents staining intensity. The DNA fragmentation cells showed in R₁ block diagram. (B) Gene expression of Caspase 3. (C) Gene expression of Bcl 2. The value represents the mean \pm standard deviation of three replicates. The asterisks * $p \leq 0.05$, ** $p \leq 0.001$ comparing the untreated with treated (various AgNPs and Ag+) cells.

Figure 5. Biodistribution of AgNPs in different tissues. Mice were exposed to (controls), citrate AgNPs, PEG AgNPs, PVP AgNPs, BPEI AgNPs and Ag⁺ by intravenously injection for 24 h. Liver, spleen, lung, kidney, gut and brain were then harvested and concentration of Ag was determined using ICP-MS. (A) Tissue weight total silver amount per gram of wet-weight. (B) Total silver amounts in various tissues. Data are expressed as means \pm standard deviation ($n = 5$).



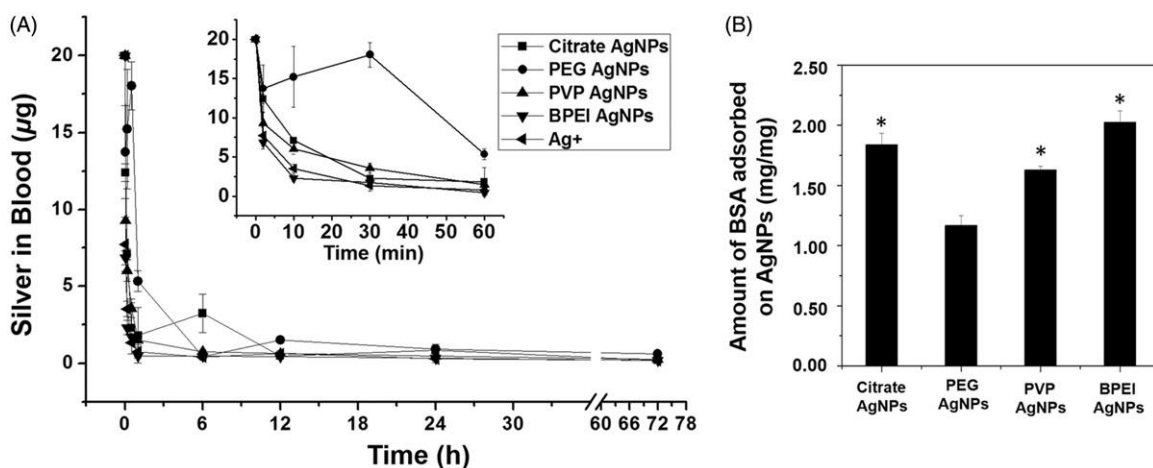


Figure 6. Pharmacokinetics of AgNPs in mice and adsorption ability of BSA by AgNPs. (A) The total blood silver as a function of time in mice. Citrate AgNPs, PEG AgNPs, PVP AgNPs, BPEI AgNPs and Ag⁺ were injected into mice via a tail vein at a dose of 1 mg Ag/kg body weight per mouse (i.e. 20 mg Ag per mouse), respectively. Five mice were used at each time point. Data are expressed as means \pm standard deviation ($n=5$). (B) Amount of BSA adsorbed on Citrate AgNPs, PEG AgNPs, PVP AgNPs and BPEI AgNPs. PEG AgNPs showed lower protein adsorption. The amount of BSA adsorbed on Citrate AgNPs, PVP AgNPs and BPEI AgNPs are significant higher than PEG AgNPs. Data are expressed as means \pm standard deviation ($n=3$). The asterisks *represent $p \leq 0.05$ when compared PEG AgNPs with Citrate AgNPs, PVP AgNPs, BPEI AgNPs groups.

Table 2. Pharmacokinetics parameters of silver in blood after injection of AgNPs via tail vein for 72 h in mice.

Parameters	Two compartment model				Non-compartment model
	Citrate AgNPs	PVP AgNPs	BPEI AgNPs	Ag ⁺	PEG AgNPs
AUC (h.mg/g)	39.18	9.45	7.90	13.91	59.13
$t_{1/2}$ (h)	0.11	0.02	0.05	0.10	51.65 ^a
$t_{1/2}^{\beta}$ (h)	17.81	3.03	6.76	15.79	–
CL (g/h)	0.51	2.12	2.53	1.44	0.23
CLD2(g/h)	10.14	37.90	30.72	19.20	–
V _{ss} (g)	12.66	8.86	23.24	30.87	14.18
V1(g)	2.03	1.02	3.10	3.14	–
V2 (g)	10.63	7.84	20.14	27.74	–

AUC, area under curve; $t_{1/2}$, first elimination half-life; $t_{1/2}^{\beta}$, Terminal elimination half-life; CL, central compartment clearance;

CLD2, peripheral compartment clearance; V_{ss}, volume of distribution at steady-state in the central compartment; V1, volume of distribution in central compartment; V2, volume of distribution in peripheral compartment.

^a $t_{1/2}$, elimination half-life.

Surface chemistry dependent toxicity and biodistribution of AgNPs in mice

The biodistribution results showed that the total Ag was higher in spleen and liver followed in a decreasing order by lungs, gut, kidneys and brain (Figure 5). This result is similar to other studies on Ag₂S and AgNPs distribution in Balb/c mice (Xue et al., 2012; Zhang et al., 2013) and also consistent with the general properties of NPs *in vivo*, e.g. NP mainly deposited in the organs of the reticuloendothelial systems (e.g. liver and spleen) after intravenous injection (Bae & Park, 2011; Li & Huang, 2008; Owens & Peppas, 2006). In addition, the size of the AgNPs (30 nm) used in our study, that is smaller than pore size of liver fenestrates (ca. 100 nm), also contributed to the enhanced liver uptake.

Moreover, mice exposure to various AgNPs also showed different body burdens, e.g. the highest body burden for BPEI AgNPs in the lung and for PEG AgNPs in the spleen. The high body burden of BPEI AgNPs in the lung may be due to the positive surface charge of AgNPs that can form aggregates in the presence of the negatively charged serum protein once injected intravenously. The large aggregated particles often cause transient embolism in the lung capillaries and then followed by redistribution to the liver (Zhang et al., 2005). Therefore, in our study the BPEI AgNPs exhibited a rapid blood clearance phase, with a large dose accumulating in the lung and the liver (Figures 5 and 6, Table 2). However, the mice treated with PEG AgNPs showed very high body burden in spleen (34.33 mg Ag/g spleen; 2.06 mg per mouse spleen). Similar results were also shown by Peracchia et al. (1999). The results indicated that the high spleen PEG AgNPs uptake is highly dependent on the PEG coating because near neutral potential value, hydrophilic and steric repulsion of PEG can effectively prevent the opsonin–NPs interaction and prolong blood half-life of NPs, which could reach other mono-nuclear phagocyte system, such as the spleen (Li & Huang, 2008). The high body burden of PEG AgNPs in spleen and BPEI AgNPs in lung did not induce significant pathological changes based on the histopathology analysis (Supplementary Figure S4 and Table S2), indicating that the damage of AgNPs to mice was not directly relevant to the bioaccumulation of AgNPs in tissues and suggesting that PEG AgNPs could be used in splenic targeting of drug delivery.

The Ag elimination from organs was very high 24 h after intravenous injection and it was Ag type dependent. The recovered percentage of the cumulative dose for AgNPs was 16.12% (Citrate AgNPs), 31.12% (PEG AgNPs), 20.10% (PVP AgNPs) and 22.30% (BPEI AgNPs), respectively (Supplementary Table S1). Similar high elimination of AgNPs (size 20 nm, the surface coating is unknown) in rats after 2 days intravenous injection was also shown by Lankveld et al. (2010). A possible explanation may be the Ag elimination into the urine/fecals or distribution of Ag to other organs not evaluated in the study such as muscles, skin, bone and lymph nodes. The distribution of AgNPs in these organs was indeed observed in rats (Ji et al., 2007; Li et al., 2014; Takenaka et al., 2001). Overall, the biodistribution and elimination of AgNPs in mice indicated that the hydrophilic and flexible polymers on the surface of AgNPs can prevent the opsonin–NPs interaction and prolong the circulation time of the NPs in blood with an increased chance of accumulation in organs. This conclusion was further shown by the pharmacokinetics results of AgNPs in mice.

The pharmacokinetics results show that the elimination half-life of PEG AgNPs in blood was much higher than other AgNPs and Ag⁺ treatments. This finding demonstrated that the PEG coating can effectively contribute to prolong the circulation time of AgNPs in blood. In addition, our study showed different elimination half-life (elimination half-life 1 min to 52 h to various AgNPs and Ag⁺) compared to other studies (elimination half-life 15.6 h, 15 nm with unclear surface coating AgNPs) (Xue et al., 2012). The difference may be due to the different size and coating of AgNPs used in the two studies. Furthermore, the AUC was also much higher in PEG AgNPs than Citrate AgNPs, PVP AgNPs, and BPEI AgNPs and Ag⁺, respectively. Similar results were also reported by other groups (Crosasso et al., 2000; Owens & Peppas, 2006; Sadzuka et al., 1998). The high AUC may be due to the fact that the surface of PEG AgNPs provided optimal biological inertia of AgNPs that resisted opsonization or non-specific binding to proteins in mice (Boulos et al., 2013; Chung et al., 2008; Huang et al., 2014; Yogasundaram et al., 2012; Zhang et al., 2013). To support this hypothesis, adsorption BSA ability of AgNPs with different surface coating was performed.

The comparison of BSA adsorption for different AgNPs is shown in Figure 6(B). It clearly indicates that PEG AgNPs showed lower protein adsorption than other AgNP particles ($p < 0.05$). This result also demonstrates that the surface coating of PEG on AgNPs can diminish opsonization and therefore can heavily reduce uptake of AgNPs into cells (Figure 3A and C). Fleischer and Payne (2014) found that the cellular binding of the BSA–NP complexes is relevant to the surface charge of the NPs. The cellular binding of BSA–NP complexes depends on the surface charge of the NPs is enhanced, whereas the cellular binding of BSA–NPs complexes by anionic NPs is inhibited. Their finding helped to explain why the PEG AgNPs showed different pharmacokinetics compared to other AgNPs in our study. The injection of AgNPs with different surface coatings and surface charges formed protein–NPs, interacting differently with mouse cells and tissues.

Conclusions

Our study demonstrated that the surface charge and surface polymer played an important role in the *in vivo* and *in vitro* toxicity, biodistribution and pharmacokinetics of AgNPs. The positive surface charge of BPEI AgNPs resulted in the highest toxicity to cells and mice. The nearly neutral PEG-coated AgNPs showed low toxicity and long half-life in blood, indicating a high potential for application in drug delivery. Moreover, our findings provided an important reference for identification of AgNPs specific uncertainty factors for performing Risk Assessment of AgNPs. The *in vitro* toxicity of AgNPs was consistent with the results of the *in vivo* studies, which suggested an *in vitro* model using Hepa1c1c7 cell line connection with uncertainty factor in the risk assessment of AgNPs to reduce *in vivo* testing. To better understand the relationships between AgNPs and toxicity, future research should focus on the effects of released Ag⁺ from AgNPs with different surface coatings and find sensitive biomarkers of the AgNPs toxicity with different surface coatings. This information will allow us to perform risk assessment of AgNPs and will be useful for making choices of AgNPs exploitation in drug delivery applications.

Acknowledgements

We thank Prof. Vicki Stone and Prof. Igor Linkov for improving the manuscript and Dr. Jiefang Sun, and Dr. Zhe Wang, as well as Molecular and Environmental Toxicology Group help for technical support.

Declaration of interest

This work was funded by the National Science Foundation of China (Grant No. 21277168, 21321004, 21407162), Strategic Priority Research Program of the Chinese Academy of Sciences (XDB14030401, XDB14030402), National Program on Key Basic Research Project (973 Program) (Nos. 2010CB933500 and 2011CB933401), the National Science Fund for Distinguished Young Scholars (Grant No. 11425520), Beijing Natural Science Foundation (No. 2152037), the China Postdoctoral Science Foundation Project (No. 2013M541056) and the European Union Seventh Framework Programme (Grant No. 604305, SUN). The authors report no conflicts of interest. The authors alone are responsible for the content and writing of the paper.

References

- Bachler G, von Goetz N, Hungerbuhler K. 2013. A physiologically based pharmacokinetic model for ionic silver and silver nanoparticles. *Int J Nanomed* 8:3365–82.
- Bae YH, Park K. 2011. Targeted drug delivery to tumors: myths, reality and possibility. *J Control Release* 153:198–205.
- Boulos SP, Davis TA, Yang JA, Lohse SE, Alkilany AM, Holland LA, Murphy CJ. 2013. Nanoparticle–protein interactions: a thermodynamic and kinetic study of the adsorption of bovine serum albumin to gold nanoparticle surfaces. *Langmuir* 29:14984–96.
- Chen R, Huo LL, Shi XF, Bai R, Zhang ZJ, Zhao YL, et al. 2014. Endoplasmic reticulum stress induced by zinc oxide nanoparticles is an earlier biomarker for nanotoxicological evaluation. *ACS Nano* 8: 2562–74.
- Chung YC, Chen IH, Chen CJ. 2008. The surface modification of silver nanoparticles by phosphoryl disulfides for improved biocompatibility and intracellular uptake. *Biomaterials* 29:1807–16.
- Cronholm P, Karlsson HL, Hedberg J, Lowe TA, Winnberg L, Elihn K, et al. 2013. Intracellular uptake and toxicity of Ag and CuO nanoparticles: a comparison between nanoparticles and their corresponding metal ions. *Small* 9:970–82.
- Crosasso P, Ceruti M, Brusa P, Arpicco S, Dosio F, Cattel L. 2000. Preparation, characterization and properties of sterically stabilized paclitaxel-containing liposomes. *J Control Release* 63:19–30.
- Eom HJ, Chatterjee N, Lee J, Choi J. 2014. Integrated mRNA and micro RNA profiling reveals epigenetic mechanism of differential sensitivity of Jurkat T cells to AgNPs and Ag ions. *Toxicol Lett* 229:311–18.
- Farkas J, Christian P, Gallego-Urrea JA, Roos N, Hasselov M, Tollefsen KE, Thomas KV. 2011. Uptake and effects of manufactured silver nanoparticles in rainbow trout (*Oncorhynchus mykiss*) gill cells. *Aquat Toxicol* 101:117–25.
- Fleischer CC, Payne CK. 2014. Nanoparticle–cell interactions: molecular structure of the protein corona and cellular outcomes. *Acc Chem Res* 47:2651–9.
- Foldbjerg R, Irving ES, Hayashi Y, Sutherland DS, Thorsen K, Autrup H, Beer C. 2012. Global gene expression profiling of human lung epithelial cells after exposure to nanosilver. *Toxicol Sci* 130:145–57.
- Gaiser BK, Hirn S, Kermanizadeh A, Kanase N, Fytianos K, Wenk A, et al. 2013. Effects of silver nanoparticles on the liver and hepatocytes *in vitro*. *Toxicol Sci* 131:537–47.
- Gao H, Xiong J, Cheng T, Liu J, Chu L, Liu J, et al. 2013. *In vivo* biodistribution of mixed shell micelles with tunable hydrophilic/hydrophobic surface. *Biomacromolecules* 14:460–7.
- Gliga AR, Skoglund S, Wallinder IO, Fadeel B, Karlsson HL. 2014. Size-dependent cytotoxicity of silver nanoparticles in human lung cells: the role of cellular uptake, agglomeration and Ag release. *Part Fibre Toxicol* 11:11.

- Holder IA, Durkee P, Supp AP, Boyce ST. 2003. Assessment of a silver-coated barrier dressing for potential use with skin grafts on excised burns. *Burns* 29:445–8.
- Huang R, Carney RP, Ikuma K, Stellacci F, Lau BL. 2014. Effects of surface compositional and structural heterogeneity on nanoparticle–protein interactions: different protein configurations. *ACS Nano* 8: 5402–12.
- Ji JH, Jung JH, Kim SS, Yoon JU, Park JD, Choi BS, et al. 2007. Twenty-eight-day inhalation toxicity study of silver nanoparticles in Sprague-Dawley rats. *Inhal Toxicol* 19:857–71.
- Jiang X, Foldbjerg R, Miclaus T, Wang L, Singh R, Hayashi Y, et al. 2013. Multi-platform genotoxicity analysis of silver nanoparticles in the model cell line CHO-K1. *Toxicol Lett* 222:55–63.
- Jiang X, Miclaus T, Wang L, Foldbjerg R, Sutherland DS, Autrup H, et al. 2014. Fast intracellular dissolution and persistent cellular uptake of silver nanoparticles in CHO-K1 cells: implication for cytotoxicity. *Nanotoxicology*. [Epub ahead of print]. doi:10.3109/17435390.2014.907457.
- Kim HR, Kim MJ, Lee SY, Oh SM, Chung KH. 2011a. Genotoxic effects of silver nanoparticles stimulated by oxidative stress in human normal bronchial epithelial (BEAS-2B) cells. *Mutat Res* 726:129–35.
- Kim JH, Park JS, Yang HN, Woo DG, Jeon SY, Do HJ, et al. 2011b. The use of biodegradable PLGA nanoparticles to mediate SOX9 gene delivery in human mesenchymal stem cells (hMSCs) and induce chondrogenesis. *Biomaterials* 32:268–78.
- Kovvuru P, Mancilla PE, Shirode AB, Murray TM, Begley TJ, Reliene R. 2014. Oral ingestion of silver nanoparticles induces genomic instability and DNA damage in multiple tissues. *Nanotoxicology*. [Epub ahead of print]. doi:10.3109/17435390.2014.902520.
- Lankveld DPK, Oomen AG, Krystek P, Neigh A, Troost-de Jong A, Noorlander CW, et al. 2010. The kinetics of the tissue distribution of silver nanoparticles of different sizes. *Biomaterials* 31:8350–61.
- Lee YH, Cheng FY, Chiu HW, Tsai JC, Fang CY, Chen CW, Wang YJ. 2014. Cytotoxicity, oxidative stress, apoptosis and the autophagic effects of silver nanoparticles in mouse embryonic fibroblasts. *Biomaterials* 35:4706–15.
- Li SD, Huang L. 2008. Pharmacokinetics and biodistribution of nanoparticles. *Mol Pharm* 5:496–504.
- Li Y, Bhalli JA, Ding W, Yan J, Pearce MG, Sadiq R, et al. 2014. Cytotoxicity and genotoxicity assessment of silver nanoparticles in mouse. *Nanotoxicology* 8:36–45.
- Liang M, Lin IC, Whittaker MR, Minchin RF, Monteiro MJ, Toth I. 2010. Cellular uptake of densely packed polymer coatings on gold nanoparticles. *ACS Nano* 4:403–13.
- Lubick N. 2008. Nanosilver toxicity: ions, nanoparticles – or both? *Environ Sci Technol* 42:8617.
- Mahmood M, Casciano DA, Mocan T, Iancu C, Xu Y, Mocan L, et al. 2010. Cytotoxicity and biological effects of functional nanomaterials delivered to various cell lines. *J Appl Toxicol* 30:74–83.
- Majzoub RN, Chan CL, Ewert KK, Silva BF, Liang KS, Jacovetty EL, et al. 2014. Uptake and transfection efficiency of PEGylated cationic liposome–DNA complexes with and without RGD-tagging. *Biomaterials* 35:4996–5005.
- Massarsky A, Abraham R, Nguyen KC, Rippstein P, Tayabali AF, Trudeau VL, Moon TW. 2013. Nanosilver cytotoxicity in rainbow trout (*Oncorhynchus mykiss*) erythrocytes and hepatocytes. *Comp Biochem Physiol C Toxicol Pharmacol* 159C:10–21.
- NanoComposix: personal communication. Available at: <http://nanocomposix.eu/pages/contract-r-d>. Accessed on 14 March 2014.
- Nanodb.dk. Available at: <http://nanodb.dk/>. Accessed on 14 March 2014.
- Owens III DE, Peppas NA. 2006. Opsonization, biodistribution, and pharmacokinetics of polymeric nanoparticles. *Int J Pharm* 307:93–102.
- Pang C, Selck H, Banta GT, Misra SK, Berhanu D, Dybowska A, et al. 2013. Bioaccumulation, toxicokinetics, and effects of copper from sediment spiked with aqueous Cu, nano-CuO, or micro-CuO in the deposit-feeding snail, *Potamopyrgus antipodarum*. *Environ Toxicol Chem* 32:1561–73.
- Pang C, Selck H, Misra SK, Berhanu D, Dybowska A, Valsami-Jones E, Forbes VE. 2012. Effects of sediment-associated copper on the deposit-feeding snail, *Potamopyrgus antipodarum*: a comparison of Cu added in aqueous form or as nano- and micro-CuO particles. *Aquat Toxicol* 106–107:114–22.
- Park JS, Na K, Woo DG, Yang HN, Kim JM, Kim JH, et al. 2010. Non-viral gene delivery of DNA polyplexed with nanoparticles transfected into human mesenchymal stem cells. *Biomaterials* 31:124–32.
- Park JS, Yang HN, Woo DG, Jeon SY, Park KH. 2013. Poly(*N*-isopropylacrylamide-co-acrylic acid) nanogels for tracing and delivering genes to human mesenchymal stem cells. *Biomaterials* 34: 8819–34.
- Peracchia MT, Fattal E, Desmaele D, Besnard M, Noel JP, Gomis JM, et al. 1999. Stealth PEGylated polycyanoacrylate nanoparticles for intravenous administration and splenic targeting. *J Control Release* 60:121–8.
- Qiu Y, Liu Y, Wang L, Xu L, Bai R, Ji Y, et al. 2010. Surface chemistry and aspect ratio mediated cellular uptake of Au nanorods. *Biomaterials* 31:7606–19.
- Sadzuka Y, Hirotsu S, Hirota S. 1998. Effect of liposomalization on the antitumor activity, side-effects and tissue distribution of CPT-11. *Cancer Lett* 127:99–106.
- Sahu SC, Zheng J, Graham L, Chen L, Ihrle J, Yourick JJ, Sprando RL. 2014. Comparative cytotoxicity of nanosilver in human liver HepG2 and colon Caco2 cells in culture. *J Appl Toxicol* 34:1155–66.
- Sharma S, Chockalingam S, Sanpui P, Chattopadhyay A, Ghosh SS. 2014. Silver nanoparticles impregnated alginate-chitosan-blended nanocarrier induces apoptosis in human glioblastoma cells. *Adv Health Mater* 3:106–14.

- Singh RP, Ramarao P. 2012. Cellular uptake, intracellular trafficking and cytotoxicity of silver nanoparticles. *Toxicol Lett* 213:249–59.
- Suliman YA, Ali D, Alarifi S, Harrath AH, Mansour L, Alwasel SH. 2015. Evaluation of cytotoxic, oxidative stress, proinflammatory and genotoxic effect of silver nanoparticles in human lung epithelial cells. *Environ Toxicol* 30:149–60.
- Takenaka S, Karg E, Roth C, Schulz H, Ziesenis A, Heinzmann U, et al. 2001. Pulmonary and systemic distribution of inhaled ultrafine silver particles in rats. *Environ Health Perspect* 109:547–51.
- Trefry JCW, Dawn P. 2013. Silver nanoparticles inhibit vaccinia virus infection by preventing viral entry through a macropinocytosis-dependent mechanism. *J Biomed Nanotechnol* 9:1624–35.
- Treuel L, Brandholt S, Maffre P, Wiegele S, Shang L, Nienhaus GU. 2014. Impact of protein modification on the protein corona on nanoparticles and nanoparticle–cell interactions. *ACS Nano* 8:503–13.
- Verma A, Stellacci F. 2010. Effect of surface properties on nanoparticle–cell interactions. *Small* 6:12–21.
- Walkey CD, Olsen JB, Song F, Liu R, Guo H, Olsen DW, et al. 2014. Protein corona fingerprinting predicts the cellular interaction of gold and silver nanoparticles. *ACS Nano* 8:2439–55.
- Wang L, Li J, Pan J, Jiang X, Ji Y, Li Y, et al. 2013. Revealing the binding structure of the protein corona on gold nanorods using synchrotron radiation-based techniques: understanding the reduced damage in cell membranes. *J Am Chem Soc* 135:17359–68.
- Xue Y, Zhang S, Huang Y, Zhang T, Liu X, Hu Y, et al. 2012. Acute toxic effects and gender-related biokinetics of silver nanoparticles following an intravenous injection in mice. *J Appl Toxicol* 32:890–9.
- Yamamoto M, Ikada Y, Tabata Y. 2001. Controlled release of growth factors based on biodegradation of gelatin hydrogel. *J Biomater Sci Polym Ed* 12:77–88.
- Yang EJ, Kim S, Kim JS, Choi IH. 2012. Inflammasome formation and IL-1 β release by human blood monocytes in response to silver nanoparticles. *Biomaterials* 33:6858–67.
- Yin N, Liu Q, Liu J, He B, Cui L, Li Z, et al. 2013. Silver nanoparticle exposure attenuates the viability of rat cerebellum granule cells through apoptosis coupled to oxidative stress. *Small* 9:1831–41.
- Yogasundaram H, Bahniuk MS, Singh HD, Aliabadi HM, Uludag H, Unsworth LD. 2012. BSA Nanoparticles for siRNA delivery: coating effects on nanoparticle properties, plasma protein adsorption, and in vitro siRNA delivery. *Int J Biomater* 2012:584060.
- Yu SJ, Chao JB, Sun J, Yin YG, Liu JF, Jiang GB. 2013. Quantification of the uptake of silver nanoparticles and ions to HepG2 cells. *Environ Sci Technol* 47:3268–74.
- Zhang J, Nie X, Ji Y, Liu Y, Wu X, Chen C, Fang X. 2014. Quantitative biokinetics and systemic translocation of various gold nanostructures are highly dependent on their size and shape. *J Nanosci Nanotechnol* 14:4124–38.
- Zhang JS, Liu F, Huang L. 2005. Implications of pharmacokinetic behavior of lipoplex for its inflammatory toxicity. *Adv Drug Deliv Rev* 57:689–98.
- Zhang Y, Zhang Y, Hong G, He W, Zhou K, Yang K, et al. 2013. Biodistribution, pharmacokinetics and toxicology of Ag₂S near-infrared quantum dots in mice. *Biomaterials* 34:3639–46.